Fuel 95 (2012) 287–297

Contents lists available at SciVerse ScienceDirect

Fuel

journal homepage: www.elsevier.com/locate/fuel

Atomization and vaporization for flash-boiling multi-hole sprays with alcohol fuels

Wei Zeng [a], Min Xu [a,*], Gaoming Zhang [a], Yuyin Zhang [a], David J. Cleary [b]

[a] School of Mechanical Engineering, Shanghai Jiao Tong University, National Engineering Laboratory for Automotive Electronic Control Technology, Shanghai 200240, China
[b] General Motors Global Research & Development, China Science Lab., Shanghai 201206, China

ARTICLE INFO

Article history:
Received 8 July 2011
Received in revised form 23 August 2011
Accepted 24 August 2011
Available online 13 September 2011

Keywords:
Alcohol fuels
Flash-boiling spray
Structural change
Correlation
Ambient-to-saturation pressure ratio

ABSTRACT

The spray structural changes and vaporization processes for flash-boiling multi-hole sprays over a broad range of superheated conditions were investigated using Mie-scattering and Laser-induced-exciplex-fluorescence (LIEF) optical techniques. The fuel property effects were examined by characterizing *n*-hexane, methanol and ethanol fluids over a wide range of conditions consistent with that found in today's spark-ignition-direct-injection (SIDI) engines. The macroscopic spray structure was quantified using spray penetration, spray-plume width and normalized distance between spray plumes. These structural parameters were correlated to the ratio of the ambient pressure to saturation pressure (*Pa*/*Ps*) that represents the superheated degree. Three continuous regions were identified by quantifying the spray transformation with increasing superheated degree; namely the non-flash-boiling, transitional flash-boiling and flare flash-boiling regions. Two critical values of *Pa*/*Ps* were identified, where the flash-boiling and spray collapsing transitions occurred at *Pa*/*Ps* values of 1.0 and 0.3, respectively. The evaporation process was examined using the LIEF optical technique for *n*-hexane, providing the relative vapor quantity throughout the spray transformation process. The correlations of the spray structural change and extent of vaporization with increasing superheated degree provided good insight into the mechanisms responsible for the observed behaviors during flash-boiling conditions.

1. Introduction

For spark-ignition-direct-injection (SIDI) internal combustion engines, liquid fuel is directly injected into the combustion chamber providing the opportunity for charge cooling and the ability to implement a higher geometric compression ratio. The liquid fuel spray formation and characteristics depend on the breakup and atomization processes, which are governed by the forces acting on the spray jet and droplets; such as inertia force, viscous force, surface tension force, and air drag force [1]. Flash boiling will occur when injecting fuel into conditions below the saturation pressure, dramatically influence the spray characteristic. The flash-boiling phenomenon is commonly found for homogeneous-charge engine operation, such as idle, light-load and part-load conditions that implement intake-stroke fuel injection. Both experimental and numerical investigations have shown that flash-boiling sprays consist of smaller drop sizes with an accelerated vaporization process compared to non-flashing sprays [2–4], illustrating the importance of generating fundamental knowledge of these processes.

When the superheated fuel spray is exposed to sub-saturation pressure, a portion of the fuel will transition into vapor forming bubbles within the liquid. During the fuel injection process, these bubbles undergo a rapid expansion process, resulting in a prompt disintegration of bulk liquid into smaller droplets (namely prompt atomization) [5,6]. As compared to the normal liquid phase breakup caused by the forces mentioned above acting on the liquid jet surfaces, the disintegration of the liquid jet itself caused by the internal bubble expansion is an effective mechanism that enhances spray breakup. For flash-boiling sprays, therefore, the breakup and atomization mechanisms are significantly different compared to that for non-flash-boiling sprays. This paper focuses on developing empirical correlations that describe the mechanisms associated with flash-boiling sprays; expanding upon the previously developed correlations that provided a dimensionless analysis for non-flash-boiling sprays [1].

Since Brown et al. [7,8] provided an initial description of the flash-boiling atomization process in the early 1960s, a number of studies have further investigated this phenomenon. The measurements of thermodynamic properties for gasoline and alternative fuels, such as vapor pressure [9], have provided fundamental knowledge of fuel phase transition process. Optical diagnostic and simulation techniques have been implemented to characterize flash-boiling sprays under various conditions; illustrating that fluid type, temperature and ambient pressure influence the spray characteristics [10–12]. Effect of flash-boiling on one-hole spray has been reported by previous study [13]. With increasing fuel temperature or decreasing ambient pressure, the spray angle becomes wider and spray penetration decreases with increasing the

* Corresponding author. Address: No. 800 Dongchuan Road, Minhang Distinct, Shanghai 200240, China. Tel./fax: + 86 21 34206670.
E-mail address: mxu@sjtu.edu.cn (M. Xu).

0016-2361/$ - see front matter © 2011 Elsevier Ltd. All rights reserved.
doi:10.1016/j.fuel.2011.08.048

superheated degree. A smaller spray SMD is observed at higher superheated conditions. The structural behavior of the flash-boiling spray and the influence of superheated degree have also been examined for multi-hole injector [14]. More specifically, the spray-plume angle has been shown to initially increase with increasing superheated degree. When continuing to increase the superheated degree, the multiple spray plumes are found to collapses into a single-plume structure. LIEF studies [15] have illustrated that both the liquid and vapor phases collapse with increasing superheated degree, where the vapor structure collapsed more rapidly compared to the liquid plumes. These experimental investigations unveiled the important spray structural changes under flash-boiling conditions by providing visual descriptions of the spray transformation. However, the mechanisms responsible for the spray collapsing behavior over the range of superheated degrees require further investigations. These continued studies should yield quantitative dimensionless empirical correlations that describe the mechanisms associated with breakup and atomization processes for flash-boiling sprays.

This paper provides a quantitative understanding of the spray structural changes and vaporization extend over a broad range of flash-boiling conditions. The objective was to examine the conditions found in current direct-injection engines including an assessment of the fuel property effect using *n*-hexane, methanol and ethanol fluids. The spray structural and vaporization behaviors were correlated to the ratio of ambient pressure to saturation pressure (*Pa*/*Ps*) over the range of flash-boiling conditions. These data provide dimensionless correlations that describe the spray structural transformation and vaporization for the range of conditions.

2. Apparatus and laser diagnostic techniques

Fig. 1 shows the schematic of the experimental apparatus consisting of a constant pressure chamber, a fuel supply system, a fluid temperature control system, a chamber pressurization system, a vacuum system and a laser diagnostic system. A high-pressure Bosch HEDV 1.2 eight-hole injector with a nominal spray angle of 60° was used. The fuel temperature is managed using a water conditioning system, where a water jacket was designed to surround the injector and an external system conditions the water to reach the desired fuel temperature. An injector with thermal couple embedded within the nozzle tip was used to correlate the water temperature with actual fuel temperature.

Images of the illuminated sprays were captured by an instantaneous laser imaging system. The second harmonic of an Nd: YAG laser (Pulse width: 4 ns, power: 220 mJ at 532 nm, 20 mJ at 266 nm) was used for Mie-scattering experiment, while the fourth harmonic of the laser was used for LIEF measurement. A combination of a cylindrical and spherical lens was integrated to generate a laser sheet with a thickness below 1 mm. The spray was imaged using a UV lens and a CCD camera (12 bit, 1376 × 1040 resolution, and 15 fps recording rate). The fluorescence photons are magnified with an Intensified Relay Optics (IRO). The injection event, laser and camera systems were synchronized using the programmable time unit (PTU).

Mie-scattering was implemented to generate the spray structural images for *n*-hexane, methanol and ethanol fluids. The images were post-processed using our in-house image analysis code. A threshold value was designed to distinguish between the background noise and fuel spray, which was selected according to the SAE standard J2715. The spray plume width at 30 mm downstream of the injector was measured as an indicator of spray plume angle. At each condition, 15 Mie images were collected, where the spray penetration and spray-plume width were determined for each image to provide statistical information.

Specifically for *n*-hexane, laser-induced-exciplex fluorescence (LIEF) was used to provide individual structures of the liquid and vapor components. Fluorobenzene (FB) and diethyl-methyl-amine (DEMA) were introduced as tracer components within *n*-hexane. *n*-Hexane was chosen as the substitute of gasoline to provide an accurate LIEF measurement because the FB/DEMA/hexane exciplex system has shown good coevaporation based on components measurement of an evaporating droplet [16]. The liquid and vapor fluorescence images were separated with two optical bandpass filters, where the centerline wavelength/bandwidth for liquid phase filter and vapor phase filter were 365/25 nm and 289/10 nm, respectively. A relatively narrow bandwidth vapor phase filter was chosen to minimize the liquid crosstalk. The LIEF images presented in this study were corrected for laser power absorption based on the theory developed by Abu-Gharbieh et al. [15,17]. The temperature

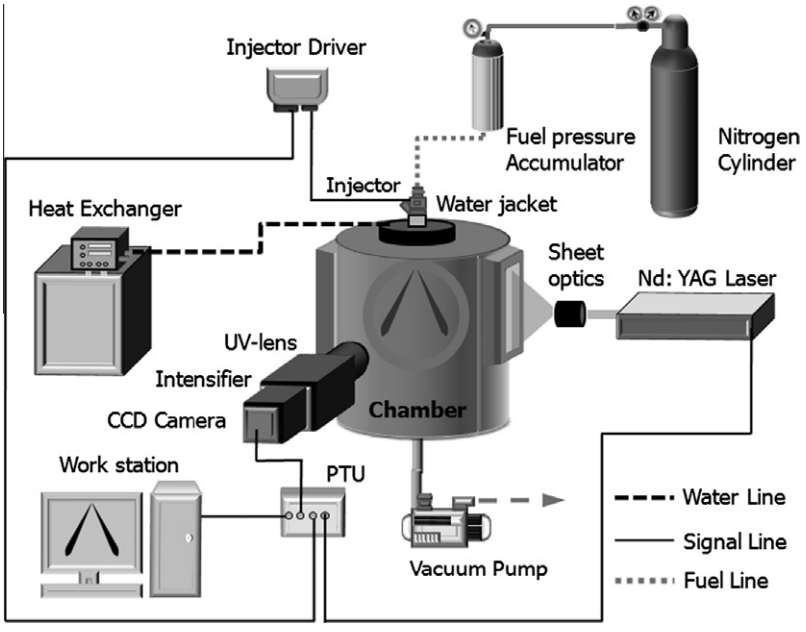

Fig. 1. Schematic of experimental apparatus.

dependence of crosstalk signal intensity for vapor image was determined and necessary corrections made. A detailed description of the LIEF technique can be found in Ref. [15,18,19].

3. Experimental conditions and fuel properties

Fig. 2a describes typical fuel pressure–temperature and in-cylinder ambient pressure conditions found in direct-injection gasoline engines. A standard commercial grade gasoline contains several hydrocarbons, typically 35–40% C5 or lower, similar levels of C6-C8 and the remainder C9-C10 hydrocarbon chains [20]. On the basis of hydrocarbon fractions of real fuel, some specific single components have been mixed to substitute the real fuel. For example, the single component fuels were chosen to be *n*-pnetane, *n*-hexane, iso-octane and o-xylene, corresponding to low, middle and high boiling-point components. In current paper, however, *n*-hexane was chosen as the substitute of gasoline to provide an accurate LIEF measurement because the fluorobenzene (FB/) diethylmethylamine (DEMA)/hexane exciplex system has shown good coevaporation. With a boiling point of 68.7 °C, the FB-DEMA-hexane mixture represents the mid-range gasoline constitutes.

In addition, the saturation curves as shown for *n*-hexane, methanol and ethanol. During the injection event, the fuel experiences a quasi-isothermal rapid expansion process. When the fuel pressure becomes below the fuel's saturation pressure, flash-boiling will occur as the formation of bubbles within the liquid core. This phenomenon occurs for lighter-load engine operating conditions and in particular at higher fuel temperatures. When fuel temperature is below 100 °C, ethanol has a lower saturation pressure compared to methanol and *n*-hexane; the ethanol spray is anticipated to experience flash-boiling at lower ambient pressures compared to the methanol and *n*-hexane sprays. For fuel temperatures between 25 °C to 50 °C, similar saturation pressures are indicated for *n*-hexane and methanol fuels while a lower saturation pressure is shown

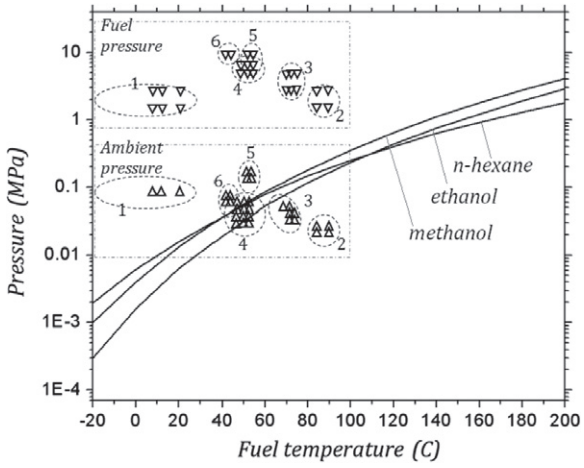

(a) Typical fuel injection and in-cylinder ambient conditions

Injection pressure (MPa)	5
Ambient temperature (°C)	25 ±1
Back pressure (kPa)	20~100
Fuel temperature (°C)	25~90
Fuel	Methanol, Ethanol, n-hexane

(b) Experimental conditions

Fig. 2. Typical fuel injection and in-cylinder ambient conditions found in direct-injection engines; regions include cold and warm operation, Idle, part-load, and wide-open-throttle conditions.

for *n*-hexane with fuel temperatures between 50 °C and 90 °C. As described in Fig. 2b, the ambient pressure and fuel temperature conditions are designed to include this entire range; where the ambient temperature and fuel pressure are maintained at 25 °C and 5 MPa, respectively. For today's DISI engines, most injection pressures are higher than 5 MPa. However, flash-boiling will occur when injecting fuel into conditions below the saturation pressure. This phenomenon mostly occurs for lighter-load engine operating conditions, such as idle and low-speed part-load. In these lighter-load operating conditions, the injection pressures are relatively lower. For example, the injection pressure for idle condition is about 2–4 MPa and for low-speed part-load is about 4–7 MPa. Therefore, the test injection was set to 5 MPa to consider the real flash-boiling conditions in DISI engines.

The physical properties at atmospheric conditions of the three fuels used in this study are shown in Table 1. The density, viscosity, and surface tension of tested methanol and ethanol fuels at fuel temperature ranging from 25 °C to 90 °C are provided in Ref. [21].

4. Results and discussions

4.1. Effect of fuel temperature, ambient pressure, and fuel type on flash-boiling spray structure

The Mie laser-sheet images for the ethanol multi-hole spray are shown in Fig. 3a, including fuel temperatures between 50 °C and 90 °C and ambient pressures between 20 kPa and 100 kPa. A dramatic spray transformation is observed where the fuel spray collapses with increasing fuel temperature and/or decreasing ambient pressure. At an ambient pressure of 40 kPa, for example, the spray penetration decreases and the spray-plume width increases when increasing fuel temperature from 50 °C to 70 °C. When the fuel temperature further increases to 90 °C, the multiple spray plumes collapse into a single mass surrounded by a large vortex of re-circulating droplets. Similar spray structural changes are observed at a fuel temperature of 70 °C when decreasing the ambient pressure from 60 kPa to 20 kPa. At an ambient pressure of 20 kPa and fuel temperature of 90 °C, a fully collapsed jet-like spray structure is observed. This dramatic structure transformation of a multi-hole spray is directly caused by the occurrence of flash-boiling [22], when the ambient pressure is reduced below the fuel saturation pressure or the temperature is above the fuel's boiling point.

A comparison of the spray structural transformation for *n*-hexane, methanol and ethanol fluids under various ambient pressure and fuel temperature conditions is shown in Fig. 3b. From these planer Mie images, the occurrence of flash-boiling is observed for each of the three fuels. However, the ethanol spray structural transformation has a delayed response to increasing fuel temperature and decreasing ambient pressure compared to that observed for the *n*-hexane and methanol sprays. A notable transformation of the *n*-hexane and methanol sprays occurred at a fuel temperature of 50 °C and ambient pressure of 40 kPa and these sprays are fully collapsed with a fuel temperature of 90 °C and ambient pressure of 100 kPa. At these same conditions, however, the ethanol spray maintains a multi-hole plume structure and only collapses at the more extreme condition with the fuel temperature of 90 °C and ambient pressure of 40 kPa.

These observed spray structural behaviors are consistent with the differences in the saturation pressure among these three fuels. At fuel temperatures between 50 °C and 90 °C, *n*-hexane and methanol sprays have similar spray structure and similar saturation pressures. The ethanol spray, however, has a lower saturation pressure and maintains a multi-hole spray plume structure until higher fuel temperature and lower ambient pressure conditions. These

Table 1
Physical properties of test fuels.

Test fuel	*n*-Hexane	Methanol	Ethanol
Surface tension (mN/m, 25 °C)	18.02	22.5	22.39
Viscosity (mPa s, 25 °C)	0.297	0.541	1.052
Density (g/mL, 25 °C)	0.655	0.784	0.782
Boiling point (°C)	68.7	64.5	78.3

data illustrate the relationship between the fuel saturation pressure to ambient pressure and fuel temperature to boiling-point temperature as the key parameters for describing the spray transformation during flash-boiling conditions.

4.2. Effect of superheated degree on spray transformation

The ratio of ambient pressure to saturation pressure (*Pa*/*Ps*) and the difference between fuel temperature and boiling-point temperature (*Tf-Tb or superheated degree*) can be used as characteristic parameters to describe the structure behaviors observed for flash-boiling sprays. Fig. 4a illustrates the specific relationships that describe the ambient-to-saturation pressure (*Pa*/*Ps)* and superheated degree (*Tf-Tb*) for *n*-hexane, methanol and ethanol fluids. A logarithmic relationship is shown indicating that these two characteristic parameters are similar in principal.

Fig. 4b compares the methanol and ethanol sprays at similar *Pa*/*Ps* values with different ambient pressures and fuel temperatures. A similar structure is illustrated when comparing these sprays at consistent *Pa*/*Ps* values. Flash-boiling is anticipated to occur at a *Pa*/*Ps* values below 1.0. At higher *Pa*/*Ps* values, for non flash-boiling sprays, the macroscopic spray structure will depend on the Weber number, Reynolds number, and the air-to-liquid density ratio [1]. With decreasing *Pa*/*Ps* values from 1.0 to 0.7, an increasing spray-plume angle and decreasing spray penetration is observed. By further decreasing *Pa*/*Ps*, the individual spray plumes are observed to collapse toward the injector centerline. At a *Pa*/*Ps* value near 0.4, the spray plumes interact and a large vortex structure is formed along the outer edge of the spray, indicating air entrainment into the spray body. When the *Pa*/*Ps* further decreases to a value of 0.3, much of the fuel mass contracts toward the injector centerline with vortexes observed along with spray edges. The spray continues to collapse into a single solid-cone plume with

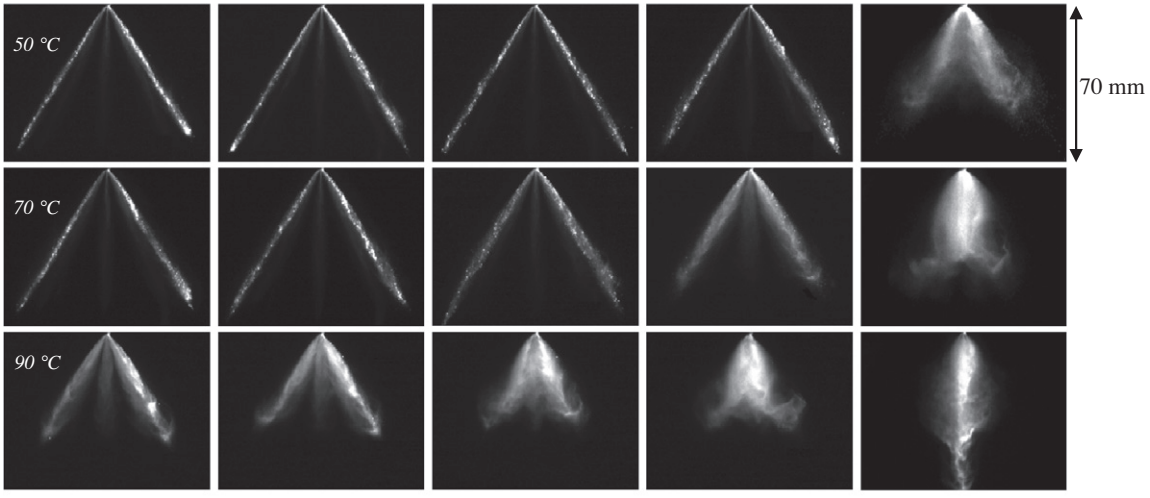

(a) Mie-scattering images of ethanol multi-hole sprays under various fuel temperature and ambient pressure conditions

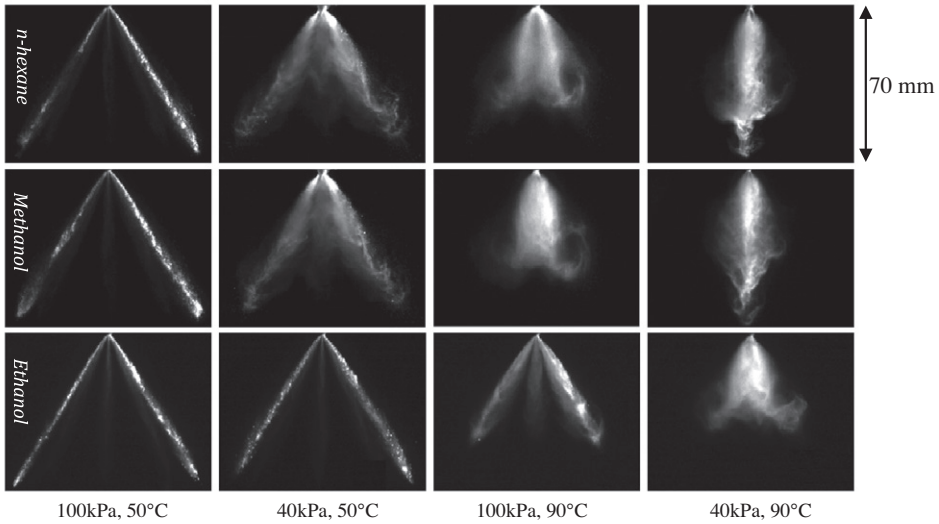

(b) effect of fuel type, fuel temperature, and ambient pressure on spray structure

Fig. 3. Ethanol multi-hole sprays under various fuel temperature and ambient pressure conditions and effect of fuel type, fuel temperature, and ambient pressure on spray structure.

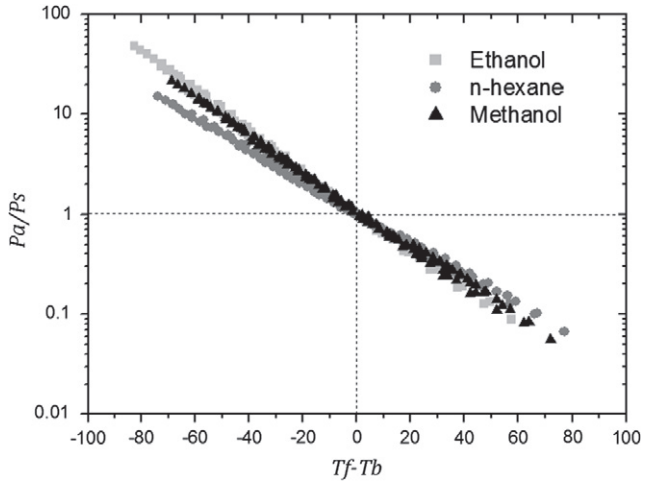

(a) Relationship between ambient-to-saturation pressure (Pa/Ps) and superheated degree (Tf-Tb)

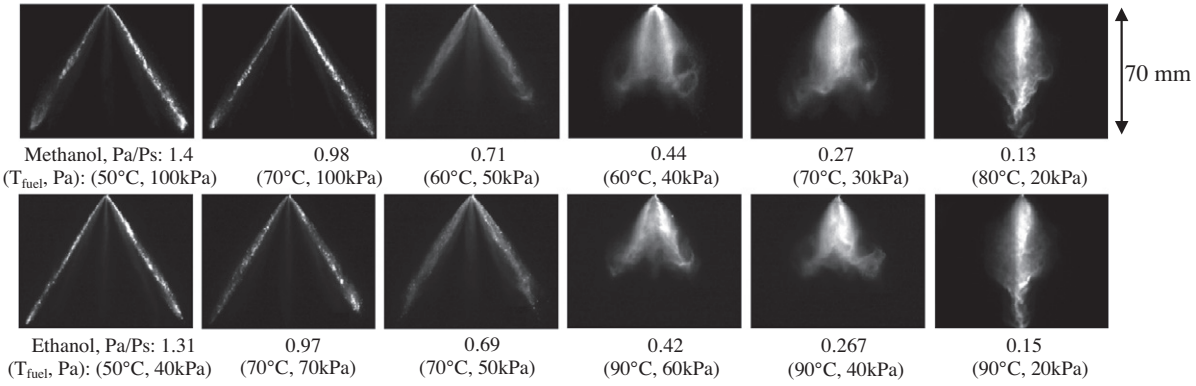

(b) effect of ambient-to-saturation pressure ratio on flash-boiling spray structure

Fig. 4. Relationship between ambient-to-saturation pressure (*Pa*/*Ps*) and superheated degree (*Tf-Tb)* and effect of ambient-to-saturation pressure ratio on flash-boiling spray structure.

sharpen spray tip and a narrowed spray cone at the *Pa*/*Ps* value of 0.15. In contrast to the previous two conditions where lower spray penetration is observed with decreasing *Pa*/*Ps*, the spray penetration substantially increased at this more extreme flash-boiling condition.

4.3. Spray structure comparison for flash-boiling and non-flash-boiling conditions

For non flash-boiling sprays, the liquid jet breakup process is dominated by competition among forces acting on the liquid jet surface [23]. The primary forces are the inertia force, surface tension force, viscous force, and aerodynamic drag force. Our previous study developed relationships between macroscopic spray characteristics and the Weber number, Reynolds number, and the air-to-liquid density ratio [1]. Good dimensionless correlations were generated that described the spray penetration and spray-plume width with generalized formulations, as summarized in Fig. 5a. These data represent a broad range of conditions found in direct-injection gasoline engines. In addition, the data for flash-boiling sprays is shown, illustrating significant variability, shorter spray penetration distance, and generally larger spray-plume width. These data demonstrate the need for generating new dimensionless correlations that describe the macroscopic structural behaviors for flash-boiling sprays.

The break-up mechanism for flash-boiling sprays must comprehend bubble formation and expansion within the bulk liquid. During the injection event, the fuel transitions from a high pressure condition to ambient pressure in a near isothermal process. When the pressure ambient reaches below the fuel saturation pressure, gaseous bubbles forms within the bulk liquid [5]. These bubbles will expand working to disintegrate the liquid into numerous small pieces and droplets. The spray breakup process, therefore, will depend on the extent of vapor generation within the nozzle.

The dimensionless ambient-to-saturation pressure ratio (*Pa*/*Ps*), an indicator of the superheated degree, is used in this study as a characteristic parameter to describe the macroscopic spray structure during flash-boiling conditions. The spray penetration and spray-plume width dependence on *Pa*/*Ps* is shown in Fig. 5b. For non flash-boiling conditions, (*Pa*/*Ps* > 1) a correlation between these macroscopic spray parameters and this dimensionless pressure ratio parameter is not observed. Under flash-boiling conditions, however, a strong relationship is shown for both the spray penetration and spray-plume angle, in spite significant differences in the Weber number, Reynolds number, and the air-to-density liquid ratio.

4.4. Dimensionless analysis of flash-boiling sprays

Fig. 6 presents additional details describing the spray penetration and spray-plume angle dependence on the ratio of ambient pressure to saturation pressure (*Pa*/*Ps*). These data include three fuels (*n*-hexane, methanol and ethanol), ambient pressures from 20 kPa to 100 kPa and fuel temperatures from 25 °C to 90 °C; providing a broad range of *Pa*/*Ps* from above 1.0 down to 0.07. Three distinct

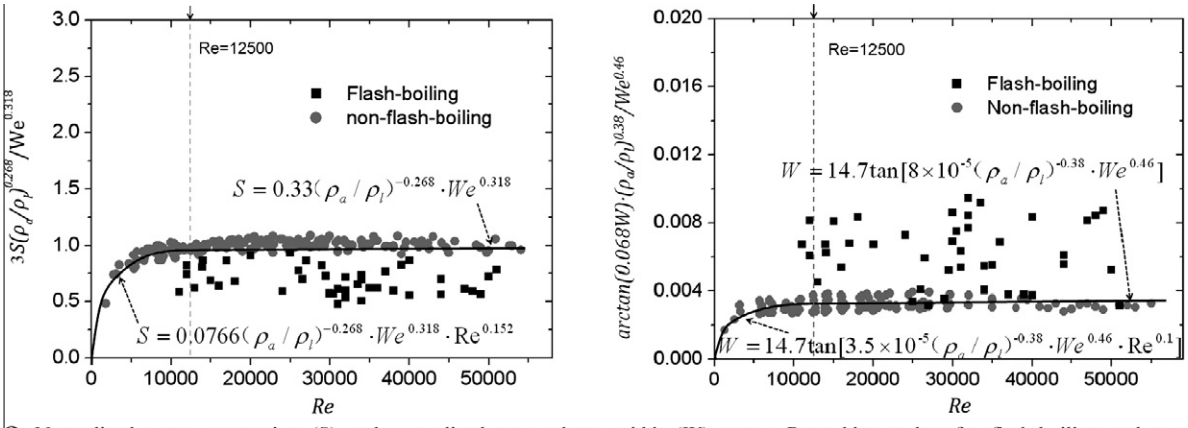

a Normalized spray penetration (S) and normalized spray-plume width (W) versus Reynolds number for flash-boiling and non flash-boiling sprays. Data provided for gasoline, methanol and ethanol.

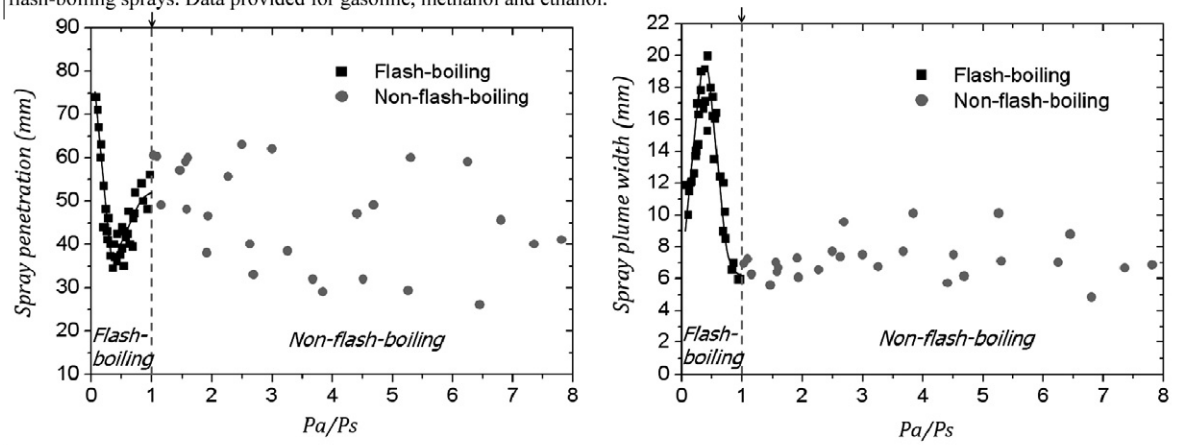

b Spray penetration and spray-plume widths versus Pa/Ps for both flash-boiling and non flash-boiling conditions; data provided for n-hexane, methanol and ethanol fuels.

Fig. 5. Spray structure comparison for flash-boiling and non-flash-boiling conditions.

regions have been defined to distinguish among non flash-boiling ($Pa/Ps > 1$), transitional flash-boiling ($0.3 < Pa/Ps < 1$), and flare flash-boiling conditions ($Pa/Ps < 0.3$). The spray break-up mechanism transitions from depending on the dynamic forces acting on the liquid surface, to a bubble formation and expansion phenomena at an ambient-to-saturation pressure ratio of 1.0. When decreasing the ambient-to-saturation pressure ratio from 1 to 0.3, the extent of vapor generated is anticipated to increase consistent with the higher superheated degree. Within this transitional flash-boiling region, a linear relationship between the spray penetration, spray-plume width, and the ambient-to-saturation pressure ratio is observed. More specifically, the spray penetration decreases and the spray-plume width increases with decreasing ambient-to-saturation pressure ratio. The individual spray plumes of the evaluated eight-hole fuel injector interact and collapse into a single-body spray at an ambient-to-saturation pressure ratio of 0.3, driving a reversal of the spray structural trends when further decreasing ambient-to-saturation pressure ratio.

In addition to the first-order ambient-to-saturation pressure ratio effect, the macroscopic spray structure has a noticeable secondary dependence on the ambient pressure for flash-boiling conditions. The spray penetration in particular increases with decreasing ambient pressure at each ambient-to-saturation pressure ratio; a direct result of lower air resistance with reduced ambient density. The air-to-liquid density ratio (ρ_a/ρ_l) is used to quantify the effect of air density on the spray penetration and spray-plume width using the following two expressions [1],

$$S \propto (\rho_a/\rho_l)^{-0.268} \tag{1}$$

$$W \propto (\rho_a/\rho_l)^{-0.38} \tag{2}$$

where S and W represent the spray penetration and spray-plume width, respectively.

The secondary effect associated with the air density is isolated by dividing the spray penetration and spray-plume width data shown in Fig. 7 by expressions (1) and (2), respectively. As presented in Fig. 7, a better correlation is observed when capturing the second-order ambient pressure contribution. The spray penetration and spray-plume width dependence on the ambient-to-saturation pressure ratio and the air-to-liquid density ratio are quantified by expressions (3) and (4) for both transitional flash-boiling and flare flash-boiling conditions. These relationships illustrate that the macroscopic spray structure can be quantitatively characterized using the ambient-to-saturation pressure ratio and the air-to-liquid density ratio only, independent of the fuel type and fuel temperature.

$$\begin{cases} S = (3.62 + 5.1\cdot Pa/Ps)\cdot(\rho_a/\rho_l)^{-0.268} & 0.3 \leqslant Pa/Ps < 1 \\ S = (9.2 - 12.45\cdot Pa/Ps)\cdot(\rho_a/\rho_l)^{-0.268} & Pa/Ps < 0.3 \end{cases} \tag{3}$$

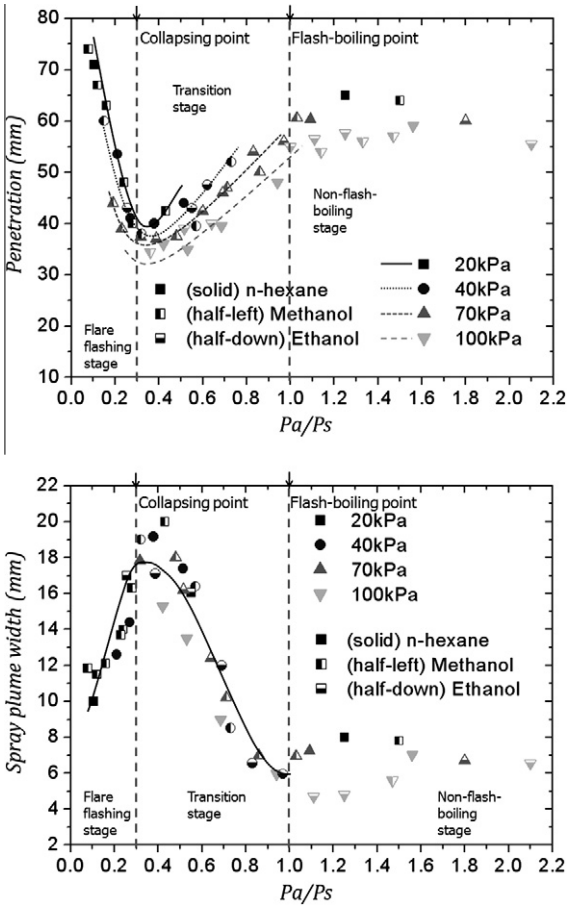

Fig. 6. Effect of *Pa*/*Ps* on spray penetration (up) and spray-plume width (bottom) under various fuel temperatures and ambient pressure conditions for *n*-hexane, methanol and ethanol fuels.

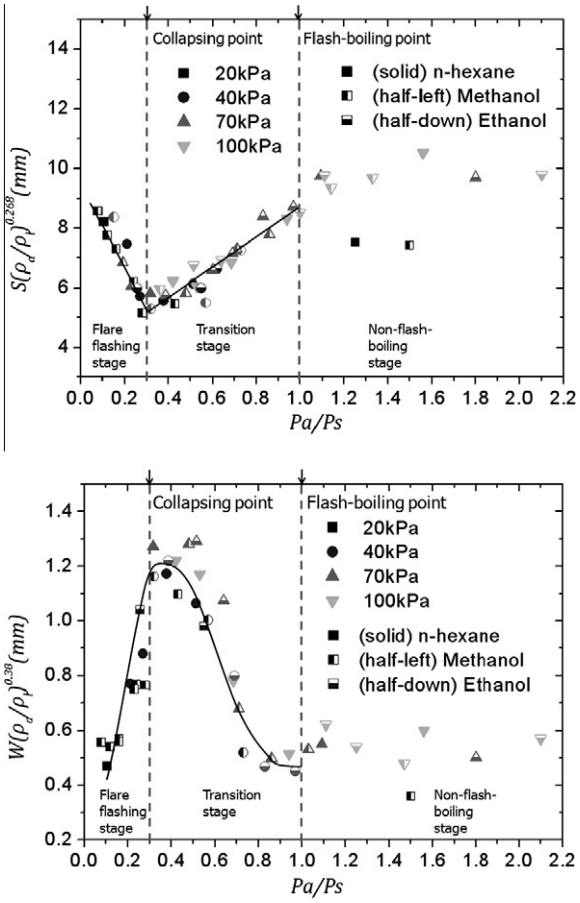

Fig. 7. Relationships describing the spray penetration (up) and spray-plume width (bottom) dependence on the ambient-to-saturation pressure ratio (*Pa*/*Ps*) and the air-to-liquid density ratio (ρ_a/ρ_l); data provided for *n*-hexane, methanol and ethanol fuels; ambient pressures between 20 kPa and 100 kPa, and fuel temperatures from 25 °C to 90 °C.

$$\begin{cases} W = \frac{1.5\cdot(\rho_a/\rho_l)^{-0.38}}{1+e^{3.8\cdot(Pa/Ps-0.746)}} & 0.3 \leqslant Pa/Ps < 1 \\ W = (9.2 - 12.45\cdot Pa/Ps)\cdot(\rho_a/\rho_l)^{-0.38} & Pa/Ps < 0.3 \end{cases} \quad (4)$$

The macroscopic spray collapsing behavior is characterized by defining a new parameter, namely, the normalized distance between two opposite spray plumes. The detailed spray structure is identified from the image intensity distribution across the spray at a distance of 30 mm downstream from the injector's tip. As an example, this image intensity distribution along with the full image at ambient-to-saturation pressure ratios of 0.97 and 0.16 is shown in Fig. 8a. At the higher ambient-to-saturation pressure ratio condition of 0.97, a bimodal distribution defines the individual spray plumes with the highest fluorescence intensity occurring near the centerline of each plume. As the ambient-to-saturation pressure ratio continues to decrease, these two individual spray plumes gradually move toward the centerline of the injector until interacting and merging into a single-plume spray. The normalized distance between the two peaks identifies the extent the spray collapse, where the individual spray-plume distance is normalized by the spray-plume distance at a fuel temperature of 25 °C and an ambient pressure of 100 kPa.

Fig. 8b presents the normalized spray plume distance for three fuels (*n*-hexane, methanol and ethanol), ambient pressures from 20 kPa to 100 kPa, and fuel temperatures from 25 °C to 90 °C. From these data, the spray collapsing behavior is determined to only depend on the ambient-to-saturation pressure ratio and does not specifically depend on the fuel type, fuel temperature, ambient pressure or air-to-liquid density ratio. The normalized distance between the individual spray plumes is constant for non flash-boiling conditions (*Pa*/*Ps* > 1). The normalized spray plume distance decreases monotonically when reducing the ambient-to-saturation pressure ratio from 1.0 down to 0.3. For ambient-to-saturation pressure ratios between 1.0 and 0.8, only a small change in the distance between the spray plumes is observed. The normalized spray plume distance decreases linearly with decreasing ambient-to-saturation pressure ratio from 0.8 to 0.3. At the spray collapsing condition, the normalized spray plume distance decreases more slowly until eventually reaching a value of zero indicating the spray has fully collapsed from a multi-plume structure to a single-plume structure. The normalized spray plume distance (D) can be quantitatively characterized by the expressions shown in Eq. (5).

$$\begin{cases} D = 1 & 0.8 < Pa/Ps \\ D = 1.665\cdot Pa/Ps - 0.32 & 0.3 \leqslant Pa/Ps \leqslant 0.8 \\ D = 0 & Pa/Ps < 0.3 \end{cases} \quad (5)$$

During flash-boiling conditions, the spray penetration, spray-plume width, and normalized distance between individual spray plumes primarily depend on the ambient-to-saturation pressure ratio. In addition, the spray penetration and spray-plume width have a second-order dependence on the air-to-liquid density ratio. With decreasing ambient-to-saturation pressure ratio below 1.0, the spray-plume width increases while the spray penetration and the distance between individual plumes decrease. These spray structural parameters continue to change in a linear fashion until the individual spray plumes interact at an ambient-to-saturation pressure ratio near 0.3. Once the individual spray plumes collapse

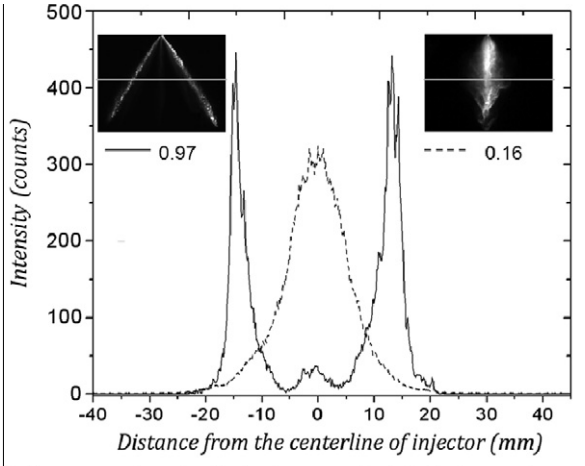

a fluorescence intensity distribution across the individual spray plumes at a distance of 30 mm from the injector's tip

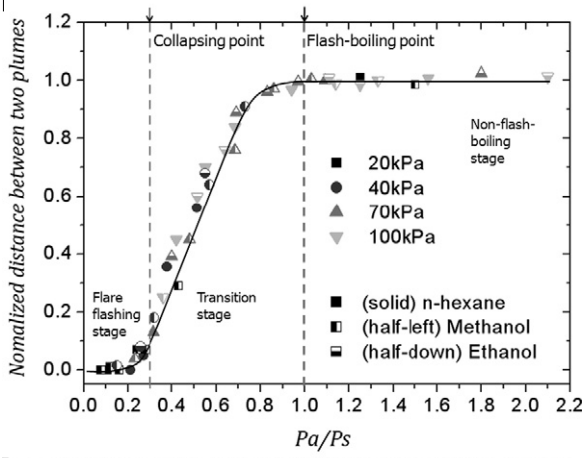

b normalized spray plume distance dependence on the ambient-to-saturation pressure ratio; data provided for n-hexane, methanol and ethanol fuels, ambient pressures between 20 kPa and 100 kPa, and fuel temperatures from 25 °C to 90 °C

Fig. 8. Intensity distribution across the individual spray plumes at a distance of 30 mm from the injector's tip and normalized spray plume distance dependence on the ambient-to-saturation pressure ratio.

into a single plume structure, the spray penetration increases and the spray-plume width decreases with decreasing ambient-to-saturation pressure; a reversal in the spray structural trends. The macroscopic structure of the flash-boiling spray, therefore, is determined to primarily depend on the ambient-to-saturation pressure ratio with a secondary dependence on the air-to-liquid density ratio. In addition, however, the interaction of individual spray plumes is found to have a dramatic influence on the spray structure illustrating the importance of identifying these separate flash-boiling regions.

4.5. Vaporization of flash-boiling sprays

Flash-boiling has a twofold effect on vaporization, first vapor bubbles generation within the liquid spray and second an enhanced vaporization process due to improved atomization. In this study, the fuel vapor characteristics are examined for *n*-hexane using the laser-induced-exciplex-florescence (LIEF) optical technique. Individual images that capture the liquid and vapor components of the spray are collected for ambient-to-saturation pressure ratios between 2.0 and 0.1, as illustrated in Fig. 9a.

Consistent with the above analysis, both the liquid and vapor components of the spray are observed to transform from a multi-hole structure to a single-plume spray as the ambient-to-saturation pressure ratio decreases from 1.0 down to 0.3. The liquid and vapor plume widths increase with decreasing ambient-to-saturation pressure ratio from 1.0 to 0.7. Also, the liquid spray penetration marginally decreases while the vapor penetration significantly increases to become more similar to the liquid spray penetration; illustrating better vaporization near the leading edge at a ambient-to-saturation pressure ratio of 0.7. The spray continues to transform with significantly larger spray-plume width and reduced spray penetration for both liquid and vapor components at an ambient-to-saturation pressure ratio of 0.45. At this condition, the spray has noticeable collapse as indicated by the smaller overall width downstream from the injector tip. The spray plumes become fully collapse to form a single body at an ambient-to-saturation pressure ratio of 0.3, where a nearly uniform liquid distribution is evident and a jet-like vapor structure is observed. Highly concentrated vapor locates centrally along the injector axis. Large vortexes are visible near the spray tip in both the liquid and vapor phases. By further reducing the ambient-to-saturation pressure ratio to 0.16, the liquid and vapor components of the spray continue to narrow resulting in a larger spray penetration.

The extent of vaporization under flash-boiling conditions is qualitatively examined using the vapor fluorescence intensity information. Fig. 9b shows the normalized integrated vapor fluorescence intensity for ambient-to-saturation pressure ratios between 0.1 and 2.0. These data were normalized by the two-dimensional integrated vapor intensity throughout the entire spray at an ambient-to-saturation pressure ratio of 1.0. For non-flash-boiling conditions ($Pa/Ps > 1$), the total vapor quantity has a relatively small dependence on the ambient-to-saturation pressure ratio. The vapor quantity increases at a higher rate with decreasing ambient-to-saturation pressure ratio during flash-boiling conditions, due to a combination of prompt thermodynamic phase transition and an enhanced atomization process. Different linear growth rates are observed for the transitional flash-boiling and the flare flash-boiling regions, which are separated by the collapsing point at an ambient-to-saturation pressure ratio of 0.3. These higher vapor concentrations can result from an accelerated vaporization process and/or increased vapor density due to the collapse of the eight individual spray plumes. While both situations are possible, an accelerated vaporization process is anticipated due to the high velocity jet-like vapor structure interacting with the liquid droplets.

4.6. Mechanisms associated with the flash-boiling spray transformation

Both the liquid and vapor components of the flash-boiling spray are subjected to dramatic changes when decreasing the ambient-to-saturation pressure ratio (increasing the superheated degree). Three distinct regions describing the flash-boiling process has been identified as summarized in Fig. 10. These regions are separated by the flash-boiling point ($Pa/Ps = 1$) and the individual spray-plume collapsing point ($Pa/Ps = 0.3$). The observed trends among the spray penetration, spray-plume angle, normalized distance between individual plumes, and the vapor quantity are anticipated to have strong inter-dependence; providing important insight into the mechanism responsible for the spray transformation.

For non-flash-boiling conditions ($Pa/Ps > 1$), the spray penetration, spray-plume width, spray-plume distance, and the vapor quantity are largely independent of the ambient-to-saturation pressure ratio. The spray-plumes are separated and characterized by small plume angles, high penetration, and relatively low vaporization. The spray breakup depends on the competition among the inertia force, surface tension force, viscous force and aerodynamic drag force acting on the liquid-jet surface. Details describing the non flash-boiling spray structure and dependence on the Weber

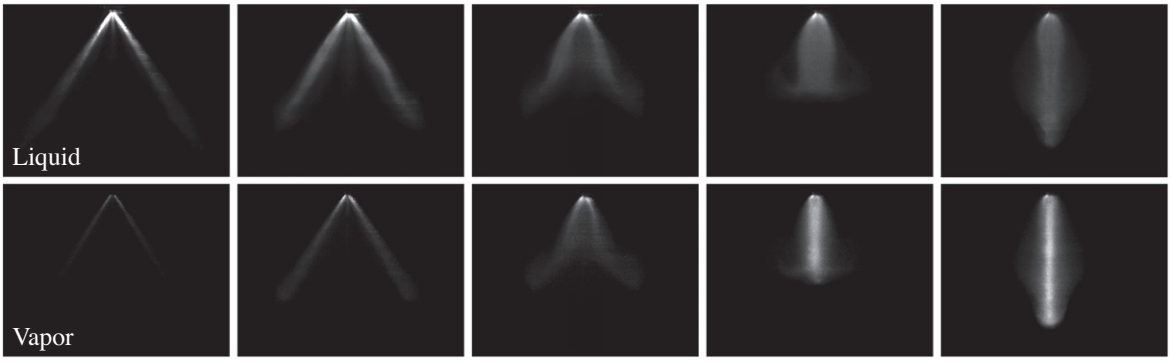

n-hexane, Pa/Ps: 1	0.70	0.45	0.3	0.16
(T_{fuel}, Pa): (25°C, 20kPa)	(52°C, 40kPa)	(62°C, 40kPa)	(72°C, 30kPa)	(75°C, 20kPa)

(a) Comparison of the liquid (top) and vapor (buttom) components of n-hexane for ambient-to-saturation pressure ratios between 0.16 and 1.0

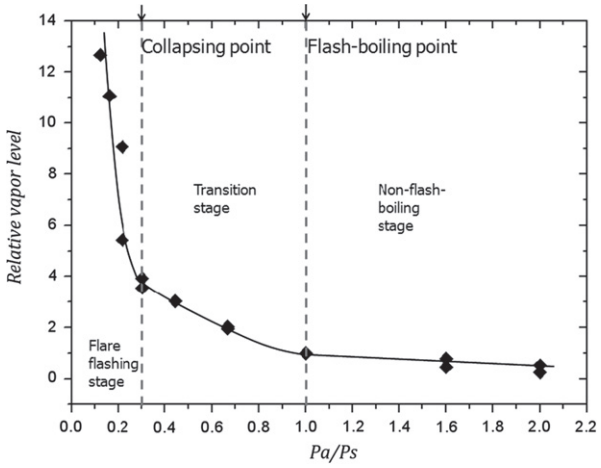

(b) Relative vapor mass dependence on ambient-to-saturation pressure ratio for non flash-boiling and flash-boiling sprays

Fig. 9. Comparison of the liquid (top) and vapor (buttom) components of *n*-hexane for ambient-to-saturation pressure ratios between 0.16 and 1.0 and relative vapor mass dependence on ambient-to-saturation pressure ratio for non flash-boiling and flash-boiling sprays.

number, Reynolds number, and the air-to-liquid density ratio can be found in Refs. [1,23].

Under flash-boiling conditions, when the ambient pressure is below the fuel's saturation pressure, vapor bubbles are formed within liquid; introducing an important mechanism that influences spray breakup. With decreasing ambient-to-saturation pressure ratio, larger vapor quantities are generated. This is not only due to the vapor formation within the bulk of superheated liquid, but also due to the enhanced superficial evaporation as a result of improved atomization. When liquid fuel enters into the nozzle, it undergoes a pressure drop from the injection pressure to the ambient pressure. In this process, vapor bubbles are formed where the local pressure is below the fuel's saturation pressure. These vapor bubbles grow as they further enter into a lower pressure region. This action of vapor bubble's formation and expansion enhances the breakup process resulting in a better atomized spray, consistent with statements [24,25] that Sauter Mean Diameter (SMD) decreases with increasing superheated degree. As a result, the trend of structural change in flash-boiling spray is different from the non-flash-boiling spray.

Within the transitional flash-boiling region ($0.3 < Pa/Ps < 1$), the vapor quantity increases with decreasing ambient-to-saturation pressure ratio (increasing superheated degree), resulting in the observed spray transformation. The spray-plume width increases with vapor quantity and decreasing ambient-to-saturation pressure ratio. The larger spray-plume width along with expected smaller droplets will reduce spray penetration due to the transformation of nozzle axial momentum (related to the penetration) to radial momentum (related to the plume-width) and due to the increase effect of the vapor and air drag forces [26].

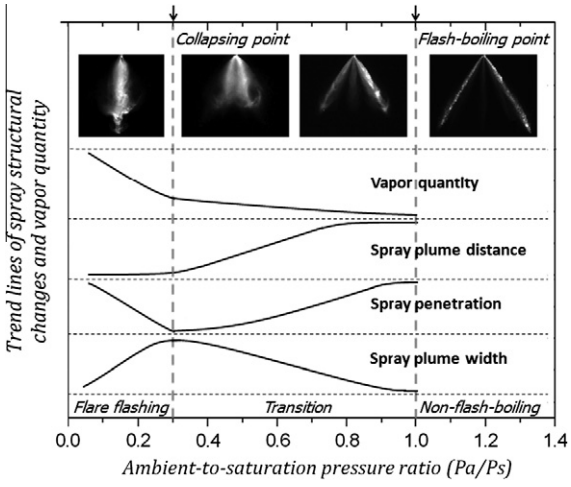

Fig. 10. Macroscopic spray structure and vapor quantity for flash-boiling sprays.

These also cause the spray-plumes to move toward the centerline of the injector with decreasing ambient-to-saturation pressure ratio. The reported normalized spray plume distance and spray penetration decreases while the spray-plume angle increases monotonically and linearly throughout much of the transitional flash-boiling region, consistent with the linearly increasing vapor quantity.

The spray plumes interact and merge into a single-body plume at an ambient-to-saturation pressure ratio of 0.3, accompanied by an apparent accelerated vaporization process. In addition, a reversal of the spray penetration and spray-plume width trends with decreasing ambient-to-saturation pressure ratio is observed. Higher spray penetration results from the higher resultant of momentum from the combining eight plumes while the radial momentum weakens due to the fully collapsing. Both the liquid and vapor components of the spray are determined to collapse into single plume, where the liquid component is uniformly distributed and the vapor component forms a jet-like structure with a centerline on the injector axis.

5. Conclusions

The macroscopic structural behaviors for a multi-hole flash-boiling spray over a broad range of superheated conditions were investigated using planar Mie-scattering and laser-induced-exciplex-fluorescence (LIEF) techniques. The effects of fuel properties were examined using *n*-hexane, methanol and ethanol fluids. The ambient-to-saturation pressure ratio (*Pa*/*Ps*), representing the superheated degree, was identified as the primary dimensionless parameter for describing spray structural characteristics and vapor quantity. The study provides insight to the primary mechanism responsible for the observed spray transformation under flash-boiling conditions. By increasing the fuel temperature or decreasing the ambient pressure, it has been proven that resulted flash-boiling sprays or superheated sprays are able to improve the evaporation of the fuel spray tremendously and increase spray angle for rapid fuel–air mixing. These sprays are quite attractive for today's direct-injection engines. The conclusions are as follows:

(1) The dimensionless numbers used to describe non-flash-boiling spray breakup are inadequate to describe flash-boiling sprays; namely the Reynolds number, Weber number, and air-to-liquid density ratio. The ambient-to-saturation pressure ratio (*Pa*/*Ps*), representative of the superheated degree, is identified as the primary dimensionless number that describes the spray transformation under flash-boiling conditions.
(2) Three distinct regions describing the macroscopic spray structure has been identified; specifically, the non flash-boiling region, transitional flash-boiling region, and flare flash-boiling region. These regions are separated by the flash-boiling point ($Pa/Ps = 1$) and the spray-plume collapsing point ($Pa/Ps = 0.3$).
(3) Within the transitional flash-boiling region, the spray penetration decreases and the spray-plume angle increases with decreasing ambient-to-saturation pressure ratio. In addition, the distance between two opposite spray plumes decreases by transitioning toward the centerline of the injector. The initial observable spray-plume transformation occurred at an ambient-to-saturation pressure ratio near 0.8. Below this value, the spray penetration and the distance between spray plumes decrease linearly with the ambient-to-saturation pressure ratio until the individual spray plumes collapse into a single structure.
(4) During flash-boiling conditions, the spray penetration and spray-plume width have inverse trends with decreasing ambient-to-saturation pressure ratio. Within the transitional flash-boiling region, the spray penetration decreases while the spray-plume width increases with decreasing ambient-to-saturation pressure ratio. Within the flare flash-boiling region, the spray penetration increases while the spray-plume angle decreases with decreasing ambient-to-saturation pressure ratio.
(5) The vapor quantity linearly increases with decreasing ambient-to-saturation pressure ratio for flash-boiling conditions. The linearly dependence has a significantly larger rate within the flare flash-boiling region compared to that observed within the transitional flash-boiling region.
(6) Both the liquid and vapor components of the flash-boiling spray are subjected to dramatic changes when decreasing the ambient-to-saturation pressure ratio (increasing the superheated degree). The observed trends among the spray penetration, spray-plume angle, normalized distance between opposite plumes, and the vapor quantity are anticipated to have strong inter-dependence.

Acknowledgement

The research was carried out at National Engineering Laboratory for Automotive Electronic Control Technology in Shanghai Jiao Tong University, and sponsored by General Motors Company and National Natural Science Foundation of China (No. 51076093 / E060702).

References

[1] Zeng W, Xu M, Zhang Y. Dimensionless evaluation for direct-injection multi-hole sprays. In: Proceedings of ILASS–Asia, Kenting, Taiwan; 2011.
[2] She J. Experimental study on improvement of diesel combustion and emission using flash boiling injection. SAE paper no. 2010-01-0341; 2010.
[3] Chang DL, Lee CF. Development of a simplified bubble growth model for flash boiling sprays in direct injection spark ignition engines. P Combust Inst 2005;30:2737–44.
[4] Park BS, Lee SY. An experimental investigation of the flash atomization mechanism. Atomiz Spray 1994;4:159–79.
[5] Sher E, Bar Kohany T, Rashkovan A. Flash-boiling atomization. Prog Energy Combust Sci 2008;24:417–39.
[6] Lee J, Madablushi R, Fotache S, Gopalakrishnan S, Schmidt D P. Flashing flow of superheated jet fuel. P Combust Inst 2009;32:3215–22.
[7] Brown R, York JL. Sprays formed by flashing liquid jets. ALCh E J 1962;8:149–53.
[8] Reitz RD. A photographic study of flash-boiling atomization. Aerosol Sci Tech 1990;12:561–9.
[9] Balatin RM, Syunyaev RZ, Karpov SA. Molar enthalpy of vaporization of ethanol–gasoline mixtures and their colloid state. Fuel 2007;86:323–7.
[10] Vanderwege BA, Hochgreb S. The effect of fuel volatility on sprays from high-pressure swirl injectors. In: Twenty-Seventh symposium on combustion. Colorado, US; 1998. p. 1865-71.
[11] Vieir MM, Simoes Moreira JR. Low-pressure flashing mechanisms in iso-octane liquid jets. J Fluid Mech 2007;572:121–44.
[12] Serras Pereira J, Van Romunde Z, Aleiferis PG, Richardson D, Wallace S, Cracknell RF. Cavitation, primary break-up and flash boiling of gasoline, iso-octane and *n*-pentane with a real-size optical direct-injection nozzle. Fuel 2010;89:2592–607.
[13] Kawano D, Goto Y, Odaka M, Senda J. Modeling atomization and vaporization processes of flash-boiling spray. SAE paper no. 2004-01-0534; 2004.
[14] Zhang M, Xu M, Zhang Y, Zhang G. High-speed PIV evaluation of fuel sprays under superheated conditions. In: Proceedings of ILASS–Asia, Jeju, Korea; 2010.
[15] Zhang G, Xu M, Zhang Y, Zhang M, Cleary D. Macroscopic characterization of flash boiling sprays using laser induced exciplex fluorescence from a multi-hole DI injector. In: Proceedings of ILASS–Asia, Jeju, Korea; 2010.
[16] Ghandhi JB, Felton PG, Gajdeczko BF, Bracco FV. Investigation of the fuel distribution in a two-stroke engine with an air-assistant injector. SAE paper no. 940394; 1994.
[17] Abu-Gharbieh A, Persson LJ, Forsth M, Rosen A, Karlstrom A, Gustavsson T. Compensation method for attenuated planar laserimages of optically dense sprays. Appl Optics 2000;39:1260–7.

[18] Düwel I, Koban W, Zimmermann FP, Dreier T. Spectroscopic characterization of the fluorobenzene/DEMA tracer system for laser induced exciplex fluorescence for the quantitative study of evaporating fuel. Appl Phys B 2009;97:909–18.
[19] Fansler TD, Drake MC, Gajdeczko B, Düwel I, Koban W, Zimmermann FP, et al. Quantitative liquid and vapor distribution measurements in evaporating fuel sprays using laser-induced exciplex fluorescence. Meas Sci Technol 2009;20:125401.
[20] Aleiferis PG, Serras-Pereira J, Van Romunde Z, Caine J, Wirth M. Mechanisms of spray formation and combustion from a multi-hole injector with E85 and gasoline. Combust. Flame 2010;157:735–56.
[21] Zhu B, Xu M, Zhang Y, Zhang G. Physical properties of gasoline-alcohol blends and their influences on spray characteristics from a low pressure DI injector. In: Proceedings of ILASS–Asia, Jeju, Korea; 2010.
[22] Zeng W, Xu M, Zhang M, Zhang Y, Cleary DJ. Characterization of methanol and ethanol sprays from different DI injectors by using Mie-scattering and laser induced fluorescence at potential engine cold-start conditions. SAE paper no. 2010-01-0602; 2010.
[23] Lefebvre AH. Atomization and sprays. New York: Taylor Francis; 1989.
[24] Cleary V, Bowen P, Witlox H. Flash liquid jets and two-phase droplet dispersion I. Experiments for derivation of droplet atomization correlations. J Hazard Mater 2007;142:786–96.
[25] Witlox H, Harper M, Bowen P, Cleary V. Flashing liquid jets and two-phase droplet dispersion II. Comparison and validation of droplet size and rainout formulations. J Hazard Mater 2007;142:797–809.
[26] Vu H, Garcia Valladares O, Aguilar G. Vapor/liquid phase interaction in flare flashing sprays used in dermatologic cooling. Int J Heat Mass Trans 2008;51:5721–31.